Preprints of the 19th World Congress
The International Federation of Automatic Control
Cape Town, South Africa. August 24-29, 2014

Fuel Efficiency Analysis for Simultaneous Optimization of the Velocity Trajectory and the Energy Management in Hybrid Electric Vehicles ⋆

Gunter Heppeler * **Marcus Sonntag** * **Oliver Sawodny** *

* *Institute for System Dynamics, University of Stuttgart, Stuttgart, Germany (e-mail: {heppeler,sonntag,sawodny}@isys.uni-stuttgart.de)*

Abstract: Hybrid electric vehicles (HEV) enable higher fuel-efficiency compared to conventional vehicles. The main potential for fuel efficiency lies in the choice of torque split between the internal combustion engine and the electric motor and the gear shifting strategy. In the framework of a predictive control strategy, the vehicle velocity can be considered as another degree of freedom. To achieve minimum fuel consumption, the right choice for these three degrees of freedom over time has to be found.
In this paper, a discrete dynamic programming approach is used to find a global optimal solution for fuel efficiency potential analysis, optimizing torque split, gear shifting and velocity trajectory. For illustration, the results for a parallel hybrid electric passenger car are shown.

Keywords: Hybrid vehicles; Dynamic programming; Energy management systems; Potential analysis; Velocity optimization.

1. INTRODUCTION

Due to increasing fuel prices and stricter environmental regulations, fuel economy in cars and trucks becomes more and more important.
One approach to reduce fuel consumption is economic driving, i.e. the velocity is varied in a way that the fuel consumption is minimized. There have been several publications on this topic using different optimization approaches, e.g. dynamic programming, Hellström et al. [2010], Pontryagin's minimum principle, Petit and Sciarretta [2011]. These have been applied to identify fuel optimal driving in conventional cars and trucks (Hooker [1988], Terwen et al. [2004]), fuelcell cars (Sciarretta et al. [2004]) and electric cars (Petit and Sciarretta [2011]).
Hybrid powertrains are a different approach to increase fuel efficiency. Almost every car manufacturer is now offering hybrid cars. Due to the second energy source in hybrid vehicles, the powertrain becomes more complex. In addition to the efficient components, a good control strategy for energy sources is essential for low fuel consumption. Developing optimal control strategies has been subject to research for some time. For previous work on energy management on hybrid vehicles, see Sciarretta and Guzzella [2007], Pisu and Rizzoni [2007] and Bender et al. [2013].
Combining both hybrid powertrains and eco-driving, for example as predictive cruise control, would lead to further fuel saving potential. However, there is only limited literature on eco-driving for hybrid vehicles.

⋆ This work is part of the "Promotionskolleg Hybrid", a cooperation between science and industry, funded in part by the Ministry of Science, Research and the Arts of the State of Baden-Württemberg, Germany.

Kim et al. [2009] propose a model predictive controller optimizing both velocity profile and torque split with a gradient based optimization. The cost function for the torque split is formulated similar to the cost function in the equivalent consumption minimization strategy (ECMS) and the equivalence factor is calculated similarly to an adaptive ECMS, see for example Musardo et al. [2005]. However, this work does not take into account road grades.
In van Keulen et al. [2009] and van Keulen et al. [2010], optimal velocity profiles for parallel hybrid trucks are studied. In their work, the shape of the velocity trajectory is predefined: the route is divided into segments of constant power request, where the velocity trajectory is divided into four phases: max. power acceleration, constant velocity, coasting and max. power deceleration. The velocity trajectory is designed in order to maximize energy recovery potential, while minimizing the fuel consumption.
In Ngo et al. [2010], dynamic programming with underlying adaptive ECMS is used to obtain optimal torque split, gear shift and velocity trajectory. Gear shift and torque split are both determined by the adaptive ECMS algorithm. If charge sustainment is not achieved, the starting equivalence factor is updated iteratively.
Another work, Mensing et al. [2012], uses dynamic programming in combination with the identified energy management system (EMS) of a Toyota Prius II, thus the optimal velocity trajectory for a given EMS is obtained. Here also the battery state of charge (SoC) is taken into account in the dynamic programming, leading to charge sustainment without further iterations.
All of this work either does not optimize the EMS (van Keulen et al. [2010], Mensing et al. [2012]) or uses an instantaneous strategy where the trip information is introduced by an (adaptive) equivalence factor

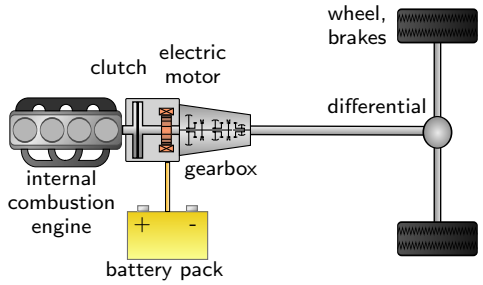

Fig. 1. powertrain configuration.

(Kim et al. [2009], Ngo et al. [2010]).
In this work, an approach for analysis of fuel efficiency potential is proposed, where torque split, gear shift and velocity trajectory are all optimized using the dynamic programming method. For details on dynamic programming, see Bertsekas [2007]. Instead of using a velocity range in combination with a constraint on the final time, the method proposed here uses a velocity range in combination with weights on the velocity deviation. With this, there is no need to include a time state and therefore computation effort is decreased. However, the final time for a driving cycle can vary for different weightings. Also, additional comfort criteria to reduce gear or engine toggling are introduced.

The paper is organized as follows: in Section 2, the vehicle model is shown. In Section 3, the optimal control problem is constructed. Simulation results are shown in Section 4 and Section 5 gives concluding remarks.

2. VEHICLE MODEL

The passenger car dealt with in this work is a parallel hybrid-electric vehicle (HEV), in which the internal combustion engine (ICE) and electric motor (EM) are separated by a clutch, see Fig. 1. In combination with electrified auxiliaries, this allows pure electric driving and coasting with both ICE and EM switched off. The ICE is a 225 kW homogenous gasoline engine. For the electrical system, a 20 kW EM in combination with a 0.8 kWh lithium-ion battery pack is used. The passenger car has an automatic gearbox.
The road data is given in form of a road grade $\gamma(s)$ and a desired velocity $v_{\mathrm{des}}(s)$ both depending on vehicle position s.
For the analysis of the driving strategy, a simple longitudinal model is sufficient. Therefore, a model similar to the one presented in Guzzella [2005] is used. The longitudinal dynamics are described as follows:

$$\dot{v} = a = \frac{1}{m_{\mathrm{eff}}} \cdot \left(F_{\mathrm{air}} + F_{\mathrm{g}} + F_{\mathrm{roll}} + F_{\mathrm{power}} - \frac{T_{\mathrm{brk}}}{r_{\mathrm{whl}}} \right), \quad (1)$$

where m_{eff} is the effective mass, consisting of the vehicle mass m and the inertia of rotational parts, e.g. axes, wheels, engine and motor. T_{brk} is the torque of the service brakes and r_{whl} is the wheel radius. F_{air} is the drag force from air resistance, F_{g} the force resulting from road grade and F_{roll} is the rolling resistance. They are given by the following equations:

$$F_{\mathrm{air}} = -C_{\mathrm{air}} \cdot v^2, \quad (2)$$
$$F_{\mathrm{g}} = -m \cdot g \cdot \sin\gamma, \quad (3)$$
$$F_{\mathrm{roll}} = -m \cdot g \cdot \mu_{\mathrm{r}}(v) \cos\gamma, \quad (4)$$

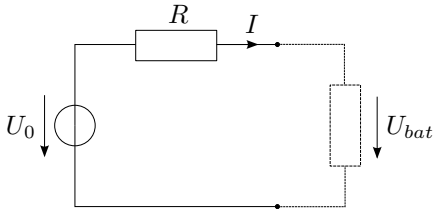

Fig. 2. Equivalent circuit model of the lithium-ion battery pack

where C_{air} is the air resistance coefficient, g is the gravity of earth and μ_{r} is the rolling coefficient given by a 1D look-up table depending on the vehicle velocity. The powertrain force F_{power} consists of all engine torques and the losses in the powertrain. It can be written as follows:

$$F_{\mathrm{power}} = \frac{1}{r_{\mathrm{whl}}} \cdot (((T_{\mathrm{ice}} + T_{\mathrm{em}} - T_{\mathrm{clt}}) \cdot i_{\mathrm{gear}} - T_{\mathrm{gear}} - T_{\mathrm{ra}}) \cdot i_{\mathrm{ra}}), \quad (5)$$

where T_{ice} and T_{em} are the ICE respectively EM torque, T_{gear} is the gearbox friction torque, depending on the torque input, gear and speed, T_{ra} is the rear axle friction torque also depending on torque at the input and speed, T_{clt} is the torque lost at the clutch, if it is open, depending on the speed difference of ICE and EM. i_{gear} and i_{ra} are the gear ratio depending on the actual gear and the rear axle ratio, the friction torques are given by look-up tables based on measurements.
For given ICE speed (ω_{ice}) and torque, the fuel consumption $\dot{m}_{\mathrm{f}}$ is given by a 2D look-up table which was identified from measurements. The same holds for the EM power consumption (P_{em}) with known speed (ω_{em}) and torque (T_{em}).
For the lithium-ion battery pack an equivalent circuit model, as shown in Fig. 2, with a state of charge (x_{SOC}) dependent voltage source U_0 and an also SoC dependent resistance R is used. For charging and discharging different resistance look-up tables R_{chg} and R_{dis} are used. For simplicity, a constant battery temperature is assumed, which is appropriate, because in the vehicle considered here the battery temperature is controlled by a cooling system to a certain temperature range.
With this the SoC derivative is

$$\dot{x}_{\mathrm{SOC}} = \frac{-I_{\mathrm{bat}}}{Q_{\mathrm{bat,max}}} = \frac{-U_0 + \sqrt{U_0^2 - 4 \cdot R \cdot (P_{\mathrm{em}} + P_{\mathrm{aux}})}}{2 \cdot R \cdot Q_{\mathrm{bat,max}}}, \quad (6)$$

where I_{bat} is the discharging current, $Q_{\mathrm{bat,max}}$ the maximum battery capacity and P_{aux} the power consumption of the auxiliaries. Note that for discharging $I_{\mathrm{bat}} > 0$ and $P_{\mathrm{em}} + P_{\mathrm{aux}} > 0$ hold.
The usable range of the SoC is restricted to the range $x_{\mathrm{SOC}} = 40\,\% \ldots 90\,\%$. Also note that high SoC values restrict the recuperation power due to the cell voltage limit.
Discrete states of the model are the actual gear $n_{\mathrm{g}} = \{0, 1, \ldots, n_{\mathrm{g,max}}\}$, the clutch state $b_{\mathrm{clt}} = \{\mathrm{open}, \mathrm{closed}\}$ and the engine state $b_{\mathrm{eng}} = \{\mathrm{on}, \mathrm{off}\}$.
With this the model has 5 states:

$$\boldsymbol{x} = [v, x_{\mathrm{SOC}}, n_{\mathrm{g}}, b_{\mathrm{clt}}, b_{\mathrm{eng}}]^T. \quad (7)$$

The torque inputs T_{ice}, T_{em} and T_{brk} are the continuous inputs to the system. Discontinuous inputs are the gear command $u_{\text{gear}} = \{0, 1, \ldots, n_{\text{g,max}}\}$, the clutch-open command $u_{\text{clt}} = \{\text{close}, \text{open}\}$ and the engine-off command $u_{\text{eng}} = \{\text{on}, \text{off}\}$. As proposed in Back [2005], for more efficient usage in dynamic programming the ICE torque T_{eng} and the brake torque T_{brk} can be combined to a generalized torque T_{gen} since braking and accelerating with the ICE at the same time is an undesired mode. Also, the gear command u_{gear} and the clutch command u_{clt} can be combined in a single input $u_{\text{g}} = \{-1, 0, 1, \ldots, n_{\text{g,max}}\}$, where -1 is the clutch-open command. Gear changing with open clutch is still possible by opening the clutch immediately after the gear change.
Hence, the input vector can be written as

$$\boldsymbol{u} = [T_{\text{gen}}, T_{\text{em}}, u_{\text{g}}, u_{\text{eng}}]^T. \tag{8}$$

3. OPTIMAL CONTROL PROBLEM

It is assumed that road slopes and desired velocities of the trip are known in advance. Note that in this work, a map position discretization is used instead of a time discretization for the optimization problem. While with time as independent variable, position would have to be included as a state, position discretization allows for omitting time as a state because the model is time-invariant. A drawback of this approach is that sections with a velocity of $0\,\text{km/h}$ can't be considered. Since this work is considering a driver assistance system, this is an acceptable limitation.
The input $\boldsymbol{u}$ is zero-order-hold discretized, which leads to

$$\boldsymbol{u}(s) = \boldsymbol{u}_k, \text{ for } s \in [s_k, s_{k+1}]. \tag{9}$$

For simplifying the notation, $\boldsymbol{x}(s_k)$ will be abbreviated with $\boldsymbol{x}_k$. The general form of an optimal control problem is the following:

$$\min_{\boldsymbol{u}} J = \min_{\boldsymbol{u}} J_{\text{N}}(\boldsymbol{x}(s_N)) + \sum_{k=0}^{N-1} \Delta J_k(\boldsymbol{x}(s), \boldsymbol{u}_k, s), \tag{10}$$

s.t.

$$\boldsymbol{x}_{k+1} = \boldsymbol{f}(\boldsymbol{x}_k, \boldsymbol{u}_k, s_k)\ \forall k \in 0, \ldots, N-1 \tag{11}$$

$$0 \geq \boldsymbol{g}(\boldsymbol{x}_k, \boldsymbol{u}_k, s_k)\ \forall k \in 0, \ldots, N, \tag{12}$$

where J_{N} is the terminal stage cost and ΔJ_{k} is the stage transition cost at position s_{k} and is $\boldsymbol{g}$ is the vector function of the boundaries. The function $\boldsymbol{f}$ implements a Runge-Kutta-type integration.
The main goals of the optimization are:

- minimization of fuel consumption
- small deviation from given desired velocity v_{des}
- charge sustainment over cycle

This leads to the following terminal stage cost J_N and the stage transition cost ΔJ_k :

$$J_N(\boldsymbol{x}(s_N)) = \xi_1 v_-^2(s), \tag{13}$$

$$\Delta J_k(\boldsymbol{x}(s), \boldsymbol{u}_k, s) = \int_{s_{\text{k}}}^{s_{k+1}} \frac{1}{v(s)} \Big[\dot{m}_{\text{f}}(\boldsymbol{x}(s), \boldsymbol{u}_k) + \xi_2 v_+(s) + \xi_3 v_+^2(s) + \xi_4 v_-(s) + \xi_5 v_-^2(s)\Big] \mathrm{d}s, \tag{14}$$

where ξ_i are the weights, v_- and v_+ describe the deviation from a desired value in negative respectively in positive direction:

$$v_-(s) = \max\{0, v_{\text{desired}}(s) - v(s)\}, \tag{15}$$

$$v_+(s) = \max\{0, v(s) - v_{\text{desired}}(s)\}. \tag{16}$$

This cost function can lead to undesired behavior since some degrees of freedom, namely the engine state and the gear, are not addressed. This can result in fast toggling in gear box and engine-on-off states. Another challenge is possible toggling in the engine torque due to the fuel map. This could be addressed by using the torque derivative as new input and the torque as new state, thus increasing computational time or by considerably increasing the velocity weights, thus drastically reducing possible changes in velocity. Both of these effects are undesirable. A third option to reduce engine torque toggling is weighting the deviation from the desired acceleration. With this method the effect on the velocity variance is a lot smaller, thus it is used here.
This leads to an augmented cost function in the optimal control problem:

$$\min_{\boldsymbol{u}} \overline{J} = \min_{\boldsymbol{u}} J_N(\boldsymbol{x}(s_N)) + \sum_{k=0}^{N-1} \Delta \overline{J}_k(\boldsymbol{x}(s), \boldsymbol{u}(s), s) \tag{17}$$

with

$$\begin{aligned}\Delta \overline{J}_k(\boldsymbol{x}(s), \boldsymbol{u}(s), s) &= \Delta J_k(\boldsymbol{x}(s), \boldsymbol{u}(s), s) \\ &+ \int_{s_k}^{s_{k+1}} \frac{1}{v(s)} \cdot \Big[\xi_6 |a(\boldsymbol{x}(s), \boldsymbol{u}_k, s) - a_{\text{des}}(s)| \\ &+ \xi_7 |a(\boldsymbol{x}(s), \boldsymbol{u}_k, s) - a_{\text{des}}(s)|^2 \\ &+ \xi_8 I_{\text{bat}}^2(\boldsymbol{x}(s), \boldsymbol{u}_k)\Big] \mathrm{d}s + \xi_9 b_{\text{gear shift},k} \\ &+ \xi_{10} b_{\text{engine on},k} + \xi_{11} b_{\text{clutch close},k} + \xi_{12} Q_{\text{sync},k}\end{aligned} \tag{18}$$

where $b_{\text{gear shift}}$, $b_{\text{engine on}}$ and $b_{\text{clutch close}}$ are 1 if a gear shift, engine on or clutch close event took place in the section $[s_k, s_{k+1}]$ and 0 otherwise. Q_{sync} accounts for all ICE and EM speed synchronizations during gear shifts, clutch or engine events. The battery current plays an important role for battery aging (Peterson et al. [2010]). Penalizing the battery current in the cost function therefore reduces battery aging. For comparing battery currents the C rate is used further on. The C rate is current normalized to battery capacity: a C rate of 1 is equal to the current completely discharging the specific battery within one hour.
In order to promote longer and more pure electric driving and rolling phases, the weights ξ_i for velocity and acceleration deviations could be reduced for these phases, leading to weights $\xi_i(n_{\text{gear}}(s), b_{\text{clt}}(s))$, $\forall i \in \{2, \ldots, 7\}$ depending on the gear and the clutch state. For the sake of readability, these will be refered to as state dependent weights $\xi_i(\boldsymbol{x}(s))$ from here on.
For increasing velocity variation another option is to introduce a velocity band $\{v_{\text{band},-}, \ldots, 0, \ldots, v_{\text{band},+}\}$ in which the deviation is not penalized:

$$v_{-,\text{mod}}(s) = \max\{0, v_{\text{desired}}(s) - v(s) + v_{\text{band},-}\}, \tag{19}$$

$$v_{+,\text{mod}}(s) = \max\{0, v(s) - v_{\text{desired}}(s) - v_{\text{band},+}\}. \tag{20}$$

These terms can be used to replace $v_-(s)$ and $v_+(s)$ in equation (14). Note that the deviation from the desired velocity is bounded:

$$v_{\text{lb}}(s) \leq v_{\text{des}}(s) \leq v_{\text{ub}}(s). \tag{21}$$

Table 1. Simulation scenario overview.

Scenario	fixed velocity	free velocity	$\xi_i(\boldsymbol{x})$	velocity band without weight	$\xi_8 \neq 0$
Baseline	×	–	–	–	–
Scenario 1	×	–	–	–	–
Scenario 2	–	×	–	–	–
Scenario 3	–	×	×	–	–
Scenario 4	–	×	×	×	–
Scenario 5	–	×	×	–	×

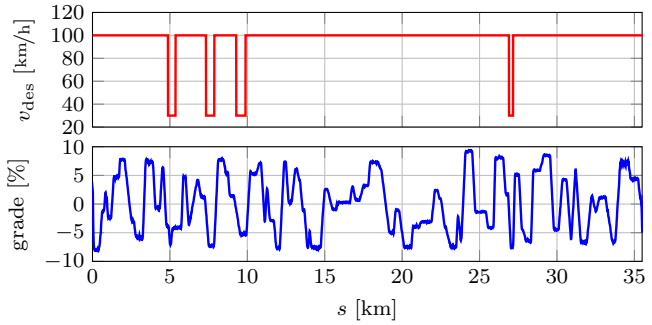

Fig. 3. Velocity and road grade used for simulation.

The bounds are defined by absolute maximum deviations from the desired velocity in each direction and in case of the upper bound also a relative maximum exceedance of the speed limit. For numerical reasons, there is also a small absolute lower bound on $v_{\text{lb}}(s)$. To guarantee charge sustainment a constraint on the final SoC is used:

$$x_{\text{SOC}}(s_N) \geq x_{\text{SOC}}(s_0). \tag{22}$$

The physical constraints on e.g. engine, motor and battery are also considered in the optimization formulation, but are omitted here.

4. RESULTS

A round trip consisting of road grade and speed limits on a country road near Ulm, Germany, is taken as driving cycle for the simulation. As shown in Fig. 3, it is a hilly road with a grade between -8 % and 9.3 %, sections with desired velocities of 100 km/h and 30 km/h and a total length of 35.6 km.

For comparison, a baseline strategy with an ECMS energy management system is used which is characterized by a fixed equivalence factor achieving charge sustainment, gear shifting look-up tables and a PI-controller following the desired velocity very closely.

For the optimal control problem (17) the following scenarios are considered (see also Table 1):

- Scenario 1: Fixed velocity profile
- Scenario 2: Variable velocity profile and constant weights ξ_i, no battery current weighting
- Scenario 3: Variable velocity profile, state dependent velocity and acceleration weights $\xi_i(\boldsymbol{x})$ (reduced for neutral gear and open clutch), no battery current weighting
- Scenario 4: Variable velocity profile, state dependent velocity and acceleration weights $\xi_i(\boldsymbol{x})$, small velocity band without weighting, no battery current weighting
- Scenario 5: Variable velocity profile, state dependent velocity and acceleration weights $\xi_i(\boldsymbol{x})$, battery current weighting

The weights ξ_i have been determined iteratively by simulations and subsequent drivability checks. They were chosen to avoid undesired behavior, like gear or engine toggling or stationary deviation from the desired velocity. For the velocity optimization a deviation of ± 8 km/h from the desired velocity is allowed. The initial conditions are always

$$s_0 = 0\,\text{km} \tag{23}$$

$$\begin{bmatrix} v(s_0) \\ x_{\text{SOC}}(s_0) \\ n_g(s_0) \\ b_{\text{clt}}(s_0) \\ b_{\text{eng}}(s_0) \end{bmatrix} = \begin{bmatrix} 100\,\text{km/h} \\ 70\,\% \\ 7 \\ 0 \\ 1 \end{bmatrix}. \tag{24}$$

The main results can be seen in Table 2.

As can be seen, the baseline scenario is far from the global optimal DP wrt. to fuel consumption and gear shifts. The constant equivalence factor needed for charge sustainment leads to a high SoC level compared to the DP solution with fixed velocity, see Fig. 4, reducing the recuperation potential due to the upper voltage of the battery pack (km 20-21, km 23-24). Another characteristic of the DP solution is the usage of overboosts (applying EM torques while ICE is at full power) to avoid down shifts (km 18-19), leading to a higher driving comfort, but also a smaller or no power reserve which is however acceptable in case of a predictive cruise controller. The torques in the figures are normalized to the maximum achievable positive and negative torques. Note that negative generalized engine torques are normalized to two times the engine drag torque due to a better visualization, thus engine torques smaller than $-\frac{1}{2}$ are service brake torques. Figure 4 also shows that the DP solution has longer phases of pure electric driving (km 19-22). A drawback of the low SoC level of the DP solution in this driving cycle is the need for active battery charging which uses additional fuel near the end of the cycle. Note that the difference in driving time is mainly due to a velocity excess in the baseline scenario at the 30 km/h sections, where the PI-controller is not able to reduce the velocity fast enough.

When also optimizing the velocity trajectory, this additional degree of freedom is mainly used to increase the numbers of pure electric driving phases or increase their length by decelerating to reduce the power demand of the vehicle. This can lead to locally different SoC trajectories and a slightly increased driving time. Further decreasing the weights for desired velocity deviation during pure electric driving or coasting in neutral gear leads to further reduction in fuel consumption, while only slightly increasing the driving time. Note that in both cases the velocity deviations mainly occur in phases where the engine is turned off which are further promoted. Note that this also leads to a more distinct use of kinetic energy thus slightly reducing the average C rate and reducing battery wear.

Since both cases are qualitatively very similar, Fig. 5 only shows a comparison between DP with fixed velocity and DP with state dependent weights $\xi_i(\boldsymbol{x})$. In this figure, several typical velocity patterns can be seen:

- Reduction of powertrain torque in front of a downhill grade while recovering velocity due to the grade without the use of fuel (see km 19)
- Gain of momentum in front of an uphill slope, using the kinetic energy to save fuel during the slope (see km 14.5, km 21)

Table 2. Simulation results: Comparison between different weighting approaches.

Scenario	Fuel consumption (normalized)	Trip duration (normalized)	Gear shifts	Engine-off to trip time ratio	Mean velocity deviation	Average C rate
Baseline	100.0 %	100.0 %	76	50.5 %	0.2 km/h	10.2
Scenario 1	98.4 %	100.1 %	16	52.9 %	0.0 km/h	11.6
Scenario 2	96.1 %	100.7 %	13	55.8 %	0.6 km/h	12.5
Scenario 3	94.1 %	100.7 %	15	62.1 %	1.1 km/h	11.3
Scenario 4	93.2 %	99.9 %	15	62.5 %	1.9 km/h	10.7
Scenario 5	93.9 %	100.2 %	21	61.0 %	1.7 km/h	6.8

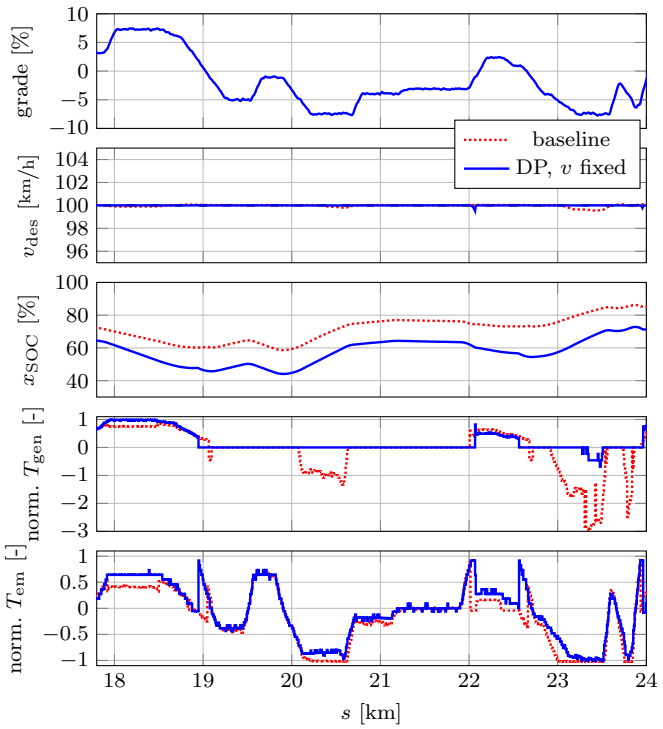

Fig. 4. Comparison of baseline scenario and DP with fixed velocity.

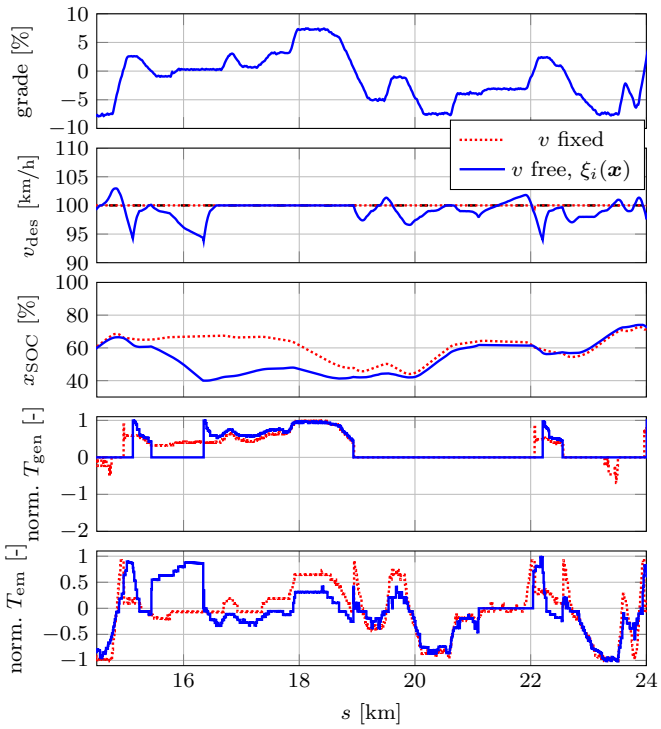

Fig. 5. Comparison of DP with fixed velocity and DP with free velocity and state dependent weights $\xi_i(\boldsymbol{x})$.

- Additional pure electric driving phase, while decelerating (see km 15.5). Although locally leading to significant fuel savings, additional fuel must be used later on to regain speed and battery charge
- Lower velocity weights also allow coasting in neutral gear (instead of recuperation, see km 21)
- When switching to a lower velocity set point, the deceleration is reduced and stretched in time to allow for more recuperation which would otherwise be missed due to recuperation power limitations (see Fig. 6).

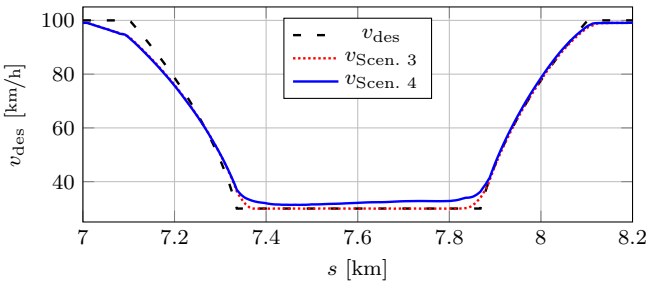

Fig. 6. Velocity trajectory in scenario 3 and 4 for changes in the desired velocity.

Including an additional band in which the velocity deviation is not penalized leads to a further increase in fuel economy. Note that a negative deviation should always be weighted, or else trip time drastically increases. For scenario 4, a velocity exceedance of up to +2 km/h is not penalized ($v_{\text{band},-} = 0$ km/h, $v_{\text{band},+} = 2$ km/h). Note that the difference in trip time is mainly due to an increased velocity of up to 33 km/h in the 30 km/h sections (see Fig. 6). The reason for this is a smaller velocity delta when accelerating back to 100 km/h. Also variation in potential and kinetic energy usage is increased and in turn usage of the electric system is slightly decreased, leading to higher velocity deviations.

All these scenarios have high average C rates in comparison to scenario 5. Penalizing the battery current allows for reducing C rates without significant increase in fuel consumption. In Fig. 7, the scenarios 3 and 5 (with and without current weight) are compared. Note that the average C rate could be drastically reduced while even achieving a slightly lower fuel consumption, compared to scenario 3, which is advantageous for battery aging (Peterson et al. [2010]). The slightly higher fuel efficiency is due to the higher average SoC level, eliminating the need for active battery charging at the end of the trip. Note that this behavior depends on the considered driving cycle. In a driving cycle with a longer recuperation phase

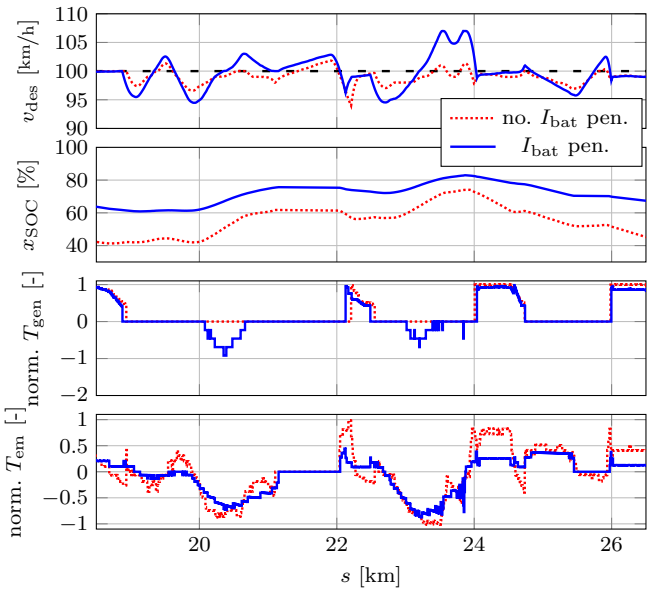

Fig. 7. Comparison of DP with free velocity and state dependent weights $\xi_i(\boldsymbol{x})$ and DP with additional current weight.

at the end, the effect on fuel efficiency may be substantially different. The chosen current penalty has high influence on the overall cost which is reducing the influence of the velocity penalties and therefore, indirectly, increases the velocity deviations by about 50 % (see Table 2), leading to a reduced driving time, but also an increasing overall cost. In Fig. 7, the typical velocity behavior described above is present in both trajectories. Note that there are only small changes in the pure electric driving phases, however active battery charging (e.g. km 22.5 and 24.5) and overboosts (e.g. km 24 and 26) are significantly reduced, leading to an increase in gear shifts. Due to the reduced influence of the velocity weights additional rolling phases in neutral gear are introduced (see km 25.5).

5. CONCLUSION

In this paper, an optimal control problem was proposed to determine the potential of a HEV operational strategy controlling gear shift, torque split, and velocity at the same time. It was shown that the additional degree of freedom for the velocity decreases fuel consumption by about 6.8 % compared to an ECMS-based strategy and about 4.3 % compared to the DP solution with fixed velocity, while only slightly increasing trip time.
Additionally, penalizing the battery current can greatly decrease the load on the battery and therefore reduce battery aging while maintaining fuel efficiency. This is due to higher deviations from the desired velocity.
The proposed approach can be used in further research to design and evaluate control algorithms combining both economic driving and energy management.

REFERENCES

M. Back. *Prädiktive Antriebsregelung zum energieoptimalen Betrieb von Hybridfahrzeugen.* PhD thesis, Universität Karlsruhe, Institut für Regelungs- und Steuerungssysteme (IRS), 2005.

F.A. Bender, M. Kaszynski, and O. Sawodny. Location-based energy management optimization for hybrid hydraulic vehicles. In *American Control Conference (ACC), 2013*, pages 402–407, 2013.

D.P. Bertsekas. *Dynamic Programming and optimal Control.* Athena Scientific, 2007.

A. Guzzella, L. & Sciarretta. *Vehicle Propulsion Systems.* Springer Berlin Heidelberg, 2005.

E. Hellström, J. Aslund, and L. Nielsen. Design of an efficient algorithm for fuel-optimal look-ahead control. *Control Engineering Practice*, 18(11):1318 – 1327, 2010.

J.N. Hooker. Optimal driving for single-vehicle fuel economy. *Transportation Research Part A: General*, 22(3): 183 – 201, 1988.

T.S. Kim, C. Manzie, and R. Sharma. Model predictive control of velocity and torque split in a parallel hybrid vehicle. In *IEEE International Conference on Systems, Man and Cybernetics, 2009. SMC 2009.*, pages 2014–2019, 2009.

F. Mensing, R. Trigui, and E. Bideaux. Vehicle trajectory optimization for hybrid vehicles taking into account battery state-of-charge. In *IEEE Vehicle Power and Propulsion Conference (VPPC), 2012*, pages 950–955, 2012.

C. Musardo, G. Rizzoni, Y. Guezennec, and B. Staccia. A-ecms: An adaptive algorithm for hybrid electric vehicle energy management. *European Journal of Control*, 11: 509 – 524, 2005.

D.V. Ngo, T. Hofman, M. Steinbuch, and A.F.A. Serrarens. An optimal control-based algorithm for hybrid electric vehicle using preview route information. In *American Control Conference (ACC), 2010*, pages 5818–5823, 2010.

S.B. Peterson, J. Apt, and J.F. Whitacre. Lithium-ion battery cell degradation resulting from realistic vehicle and vehicle-to-grid utilization. *Journal of Power Sources*, 195(8):2385 – 2392, 2010.

N. Petit and A. Sciarretta. Optimal drive of electric vehicles using an inversion-based trajectory generation approach. In *IFAC World Congress 2011*, volume 18, pages 14519–14526, 2011.

P. Pisu and G. Rizzoni. A comparative study of supervisory control strategies for hybrid electric vehicles. *IEEE Transactions on Control Systems Technology*, 15 (3):506–518, 2007.

A. Sciarretta and L. Guzzella. Control of hybrid electric vehicles. *IEEE Control Systems*, 27(2):60–70, 2007.

A. Sciarretta, L. Guzzella, and J. van Baalen. Fuel optimal trajectories of a fuel cell vehicle. In *Proceedings of AVCS 2004*, 2004.

S. Terwen, M. Back, and V. Krebs. Predictive powertrain control for heavy duty trucks. In *IFAC Symposium in Advances in Automotive Control*, 2004.

T.A.C. van Keulen, A.G. de Jager, G.J.L. Naus, M.J.G. van de Molengraft, M. Steinbuch, and N.P.I. Aneke. Predictive cruise control in hybrid electric vehicles. In *Proceedings of the 24th International Battery, Hybrid and Fuel Cell Electric Vehicle Symposium & Exhibition (EVS 24)*, 2009.

T.A.C. van Keulen, B. de Jager, D. Foster, and M. Steinbuch. Velocity trajectory optimization in hybrid electric trucks. In *American Control Conference (ACC), 2010*, pages 5074–5079, 2010.